LM -

IIT

s.)

whi

ve.

arg

w v

en (

2.(

asma

pas

This document is intended for publication in a journal, and is made available on the understanding that extracts or references will not be published prior to publication of the original, without the consent of the author.



b L loan

UKAEA RESEARCH GROUP

Preprint

VORTEX

A QUASI-STEADY SUPERMAGNETOSONIC ROTATING PLASMA EXPERIMENT

L J SRNKA

CULHAM LABORATORY
Abingdon Berkshire

CONTENTS

	Page
ITRODUCTION	1
PPARATUS	7
LASMA CURRENT-VOLTAGE CHARACTERISTICS	10
PTIMIZATION	12
RGON PLASMA FLOW CHARACTERISTICS	14
OLAR WIND SIMULATION	20
ONCLUSIONS	23
EFERENCES	25

he

1. INTRODUCTION

LEHNERT (1971) has recently reviewed rotating plasma theory and experiments. These experiments include plasma confinement and heating studies (LEHNERT et al, 1971), element and isotope separation experiments (BONNEVIER, 1971), and simulations of fuel pellet injection into fusion plasmas (ØSTER and SILLESEN, 1972). In this paper a new application for rotating plasmas is discussed. It is shown that rotating plasmas can be used as supermagnetosonic plasma wind tunnels. This development permits the experimental investigation of supersonic plasma flow problems which contain motional electric fields, i.e. a component of magnetic field transverse to the flow velocity. The interactions of bodies in the solar system with the solar wind are examples of this class of problem (SPREITER and ALKSNE, 1970).

If the azimuthal plasma flow velocity $\mathbf{v_f}$ is to be supermagnetosonic, the ions must have a minimum directed energy. The condition for supermagnetosonic flow is

$$A_{s}^{t} > A_{s}^{t} + C_{s}^{t}$$

where $v_{\rm A}$ is the Afven velocity and $C_{\rm S}$ is the plasma sound speed. This condition can be re-written for highly ionized rotating plasmas as

$$\frac{1}{2} m_i v_f^2 > \frac{1}{2} \frac{B^2}{\mu_0 n_e} + \frac{5kT_e}{2} \dots (1)$$

where m_i is the ion mass, B is the magnetic field value, μ_0 is the plasma permeability, n_e and T_e are the electron number density and temperature, respectively (assumed to be equal for ions and electrons), and k is Boltzmann's constant. The electron mass is neglected compared to the ion mass, and the ratios of specific heats for ions and electrons are both set at 5/2.

It is now known that densities $n_e \approx 5 \times 10^{20} - 1 \times 10^{21} m^{-3}$ and temperature $T_e \approx 5 - 10 \, \text{eV}$ are characteristic of high-current rotating plasma devices which have vertical magnetic fields $B_z \approx 0.1 - 0.2 \, \text{T}$ (LEHNERT, 1971). Using equation (1), these parameters require $\frac{1}{2} m_i \, v_f^2 \approx 60 - 120 \, \text{eV}$ for supermagnetosonic flow. Although this ion energy is relatively low, it is greater than the energy needed (~10-30 eV) for dissociation and single ionization of typical gases used for plasma experiments. This comparison is significant if the plasma flow interacts with neutral gas in the discharge chamber.

The use of rotating plasmas for flow studies requires flow time $\tau_f > 100 \, \mu s$ in most experiments, so that quasisteady conditions are reached. In the absence of dynamic effects (e.g. vertical pinching), this time is sufficient for plasmas with the above parameters to diffuse along B_Z to the insulating surfaces cut by the magnetic field lines (see Fig.1). Neutral layers form at such surfaces by

recombination, and balance the plasma pressure.

Results from a number of rotating plasma experiments show that v_f can be limited by a plasma-neutral gas interaction in these layers. Limitation occurs when v_f reaches a critical velocity v_c , defined by

$$\frac{1}{2} m_{i} v_{c}^{2} = e \varphi_{n}$$
 ... (2)

where e is the electron charge and ϕ_n is the ionization potential of the neutral (ALFVEN, 1954; 1960). Although this limiting effect is poorly understood, it is likely that one or more collective phenomena convert directed ion energy into thermal electron energy when $v_f \geqslant v_C \ (\text{DANIELSSON, 1970}). \ \text{Among the proposed mechanisms}$ are space-charge effects due to non-thermal ions created by symmetric resonant charge-exchange collisions, and cross-field two-stream instabilities (see the review by SHERMAN, 1969). The hot electrons ionize the wall neutrals, and the drag on the plasma rapidly increases when $v_f \geqslant v_C$ as the new ions are captured by the flow.

In experiments with uniform vertical magnetic fields, $v_f \le v_C$ everywhere in the flow if the critical velocity effect is present, since v_f is roughly constant along B_Z for typical laboratory rotating plasma conditions (LEHNERT, 1971). This effect can be observed by measuring the voltage V_T which develops radially across the plasma during the rotation. If viscosity and particle pressure

pressure gradients are ignored, then

$$V_{T} = \int_{r_{1}}^{r_{2}} E_{r} dr = -\int_{r_{1}}^{r_{2}} \left(v_{f} B_{z} + \frac{m_{i} v_{f}^{2}}{er} - \eta_{i} j_{r} \right) dr + V_{s}$$

where r_1 and r_2 are the radii to the inner and outer plasma boundaries, respectively, r is the radial position in the plasma, E_r and j_r are the radial electric field and current density, respectively, η_\perp is the electrical resistivity across B_Z , and V_S is the voltage drop across possible anode and cathode sheaths (ANGERTH et al, 1962). For most experiments, only the term containing B_Z is important. If $v_f \approx v_C$, then the critical value of V_T is

$$V_{C} = B_{Z_{O}} \left(\frac{2 e \varphi_{n}}{m_{i}} \right)^{\frac{1}{2}} (r_{2} - r_{1}) \left[1 + \frac{M^{2}}{ms} \left(1 + \frac{(r_{1} + r_{2})^{2}}{4r_{1} r_{2}} \right) \right] \dots (3)$$

provided the plasma boundaries are flux-conserving (LEHNERT, 1961; SRNKA, 1973a). Here B_{Z_O} is the initial (undisturbed) B_Z value, and $M_{ms} = v_f \cdot (v_A^2 + C_s^2)^{-\frac{1}{2}}$ is the magnetosonic mach number. Results describing V_T limitation in VORTEX are given below.

One consequence of $v_f \le v_c$ in rotating plasmas is the limitation of M_{ms} . If the ion energy required in equation (1) exceeds the limit given by equation (2), then $M_{ms} < 1$. For $M_{ms} > 1$, these two equations require

$$e \varphi_n > \frac{B_z^2}{2 \mu_0 n_e} + \frac{5kT_e}{2}$$
 ... (4)

Conversely, the number density required for a specified $m_{ms} \text{ is }$ $n_e = \frac{\left(M_{ms} B_z\right)^2}{\mu_O(2 e \phi_n - 5 k T_e M_{ms}^2)} \quad . \quad (5)$

If $2 \, \mathrm{e} \, \phi_{\mathrm{n}} < 5 \, \mathrm{kT_e} \, M_{\mathrm{ms}}^2$, then $n_{\mathrm{e}} < 0$, which means that no value of B_{Z} and n_{e} will give the desired M_{ms} . Generally, equation (5) demands high n_{e} values, as shown by the following example. For $T_{\mathrm{e}} = 1 \, \mathrm{eV}$, $\phi_{\mathrm{n}} = 13.6 \, \mathrm{V}$ (hydrogen), and $B_{\mathrm{Z}} = 0.1 \, \mathrm{T}$, $n_{\mathrm{e}} \ge 6 \times 10^{21} \, \mathrm{m}^{-3}$ for $M_{\mathrm{ms}} \ge 1$. It is difficult to produce such densities in highly ionized plasmas which have sufficient volumes and lifetimes for use in quasi-steady flow experiments.

There are two ways to produce $v_f > v_C$ and $M_{ms} > 1$ in rotating plasmas. The first approach uses a non-uniform magnetic field. If the field has a poloidal or confinement geometry (as in magnetic mirror machines), the rotational velocity increases along the field lines from $v_f \approx v_C$ at the end insulators to $v_f \approx R_r \cdot v_C$ in the midplane of the experiment. The 'radial ratio' R_r is defined as the ratio of the radial distance from the symmetry axis to a field line at the midplane, divided by the radial distance to that field line at the end insulator (i.e. $R_r \ge 1$). This geometric multiplication of v_f is due to the constant angular velocity of the field lines, and assumes the plasma is tied to the field. For this case, the ion energy requirement for $M_{ms} > 1$ in equation (4) becomes

$$e \, \phi_n > \frac{1}{R_r^2} \left(\frac{B^2}{2 \, \mu_0 \, n_e} + \frac{5kT_e}{2} \right)$$

and the density required for a specified $M_{\mbox{ms}}$ is reduced to:

$$n_e = \frac{(M_{ms} B)^2}{\mu_o (2 e R_r^2 \phi_n - 5kT_e M_{ms}^2)}$$

where B is the magnetic field value in the midplane. Velocities $v_f \approx 2-3 \, v_c$ can be produced in this way (LEHNERT, 1964), but $M_{ms} > 1$ has not been previously reported. Attempts at using larger R_r values have encountered plasma stability problems (LEHNERT, 1971).

The second approach is to reduce or eliminate the plasma/neutral gas interaction responsible for the critical velocity effect. This interaction can be avoided by introducing gas only at the midplane of the discharge chamber, through a fast valve, and then operating the discharge for a time less than the thermal diffusion time of plasma to the end insulators (HALBACH et al, 1962). Such devices have $\tau_{\rm f} < 50\,\mu{\rm s}$, which is unsuitable for some flow experiments. It may be possible to weaken the interaction by placing suitable conductors in the neutral layers, to remove any electric fields associated with the limiting effect (LEHNERT, 1969). A test of this method is in progress, but results are not yet available (LEHNERT, 1972).

Finally, it is possible to overcome the limiting effect if sufficient azimuthal force is applied to the plasma. Then the restrictions imposed by equations (4) and (5) do not apply. This approach is used in the VORTEX experiment to produce the first supermagnetosonic rotating plasma in the laboratory. Results presented by ANGERTH et al (1962) have motivated this work. It is found that $\rm M_{ms}>1\,$ can be produced in a rotating argon plasma if the radial discharge current $\rm I_T\,$ exceeds 10-15 kA, depending on the value of the magnetic field. The presence of outgassed hydrogen in the discharge chamber may help to produce $\rm v_f>v_c\,$ for argon (i.e. a 'super-critical' velocity) in this experiment.

2. APPARATUS

A schematic view of the experiment is shown in Fig.1. A homopolar configuration with $R_{\rm r}=1$ is used for simplicity (ANDERSON et al, 1958).

VORTEX has two features new to rotating plasma experiments: a narrow (0.10 m) discharge channel with a large radius of curvature, to reduce radial plasma gradients; and a preheat discharge, to give uniform starting conditions for the flow and to help prevent azimuthal current spoking.

The discharge chamber is an annular region between two cylindrical stainless steel electrodes, radii

 $r_1=0.25\,\mathrm{m}$ and $r_2=0.35\,\mathrm{m}$. These electrode walls are flux-conserving on the time scale of the plasma discharge, as recommended by MHD stability theory (MILANTIEV and ØSTER, 1969). Glass end plates seal the 0.30 m high vacuum chamber, and provide high voltage insulation. A vacuum system consisting of a rotary pump, oil diffusion pump, and a liquid-nitrogen cooled trap gives a base pressure of 2×10^{-6} torr in the chamber. A constant-flow gas system provides filling pressures p_0 in the range $5\leq p_0\leq 100\,\mathrm{mtorr}$ in a variety of gases.

Energy for the experiment is stored in three capacitor banks, which are switched using conventional ignitron techniques. The magnetic field bank drives a set of four coils, which give a vertical field $B_z = 0.01 - 0.20\,\mathrm{T}$, uniform to $\pm\,5\%$ over the discharge channel. The preheat (P.H.) and radial electric field (E_R) banks discharge into the chamber through sixteen coaxial cables, connected to a copper transmission plate and evenly spaced around the azimuth, to distribute the current uniformly.

The discharge sequence for the capacitor banks is shown in Fig.2. B_Z rises in 27 ms, and is clamped at its peak value. B_Z falls with a characteristic decay time of 91 ms after the clamp, but is essentially constant over the plasma lifetime $(0.5-1\,\mathrm{ms})$.

The preheat is an undercritically damped discharge across $\rm B_Z$, of frequency $\omega_{\rm PH}=4.8\times10^4~\rm s^{-1}$ and duration $105~\mu s$. A peak current of 140 kA is obtained at a P.H. bank voltage of 12 kV. Floating double Langmuir probe measurements show that typical P.H. parameters are $n_e=2.4\times10^{20}~\rm m^{-3}$ and $T_e=1-2~\rm eV$ at the end of the P.H. discharge, for $p_O=30~\rm mtorr$ and $B_Z=0.1~\rm T$. The ringing discharge encourages mixing and uniformity in this initial plasma, as shown by probe measurements.

The $\rm E_R$ discharge is started in the quiescent afterglow plasma of the preheat. A low-inductance series resistance in the $\rm E_R$ circuit is varied to change the $\rm E_R$ discharge characteristics. When the $\rm E_R$ waveform is undercritically damped, a clamp ignitron is used to maintain a unidirectional radial current in the plasma. The $\rm E_R$ risetime is chosen sufficiently long (~70-110 μ s) so as not to cause vertical compression or ion heating in the initial plasma (ØSTER, 1969). The decay rate for the total plasma current $\rm I_T$ is determined by the external circuit parameters if the $\rm E_R$ waveform is critically or overcritically damped, and by the plasma parameters if the discharge is undercritically damped.

Magnetic probes, high-impedance double electric probes, and floating double Langmuir probes are used for diagnostics. The Langmuir probe tips can be directed upstream, downstream,

or transverse to the flow. VARY (1970) shows that directed probes can accurately measure $\rm n_e$ and $\rm T_e$ in flowing plasmas, provided the thin-sheath approximation is valid.

3. PLASMA CURRENT-VOLTAGE CHARACTERISTICS

Discharges in hydrogen, helium, and argon were studied in VORTEX. Voltage limitation is observed in these discharges if $I_{T} \le 5 \text{ kA}$ when the E_{R} circuit is resistively damped. Typical oscillograms for a hydrogen discharge, $\rm p_{_{\rm O}} = 30\;mtorr$, $\rm B_{_{\rm Z}} = 0.1\;T$, and $\rm E_{_{\rm R}}$ bank voltage $\rm V_{_{\rm B}} = 3\;kV$, are shown in Fig.3. Oscillograms for helium and argon discharges are similar. Note that $V_{\tau \tau}$ is nearly constant while I_{T} is flowing. Increases in V_{R} do not increase $m V_{T}$, as shown in Fig.4. The dashed lines are the $m V_{C}$ values predicted from equation (3), with $M_{ms} < 1$. linear portions of the three voltage curves for demonstrate charge-sharing between the E_{R} capacitor bank and the hydromagnetic capacitance of the plasma, when ${\rm V_T} < {\rm V_C}$ (ANDERSON et al, 1959). The variation of the peak $\rm V_{\rm T}$ value with $\rm \, B_{\rm Z}$ for $\rm \, I_{\rm T} < 5 \; kA$ is shown in Fig.5, where the full and dashed lines are the predicted $\mathbf{V}_{_{\mathbf{C}}}$ values. It is also found that the peak value of $V_{\boldsymbol{T}}$ is independent of p_0 in the range $5 \le p_0 \le 100 \, \text{mtorr}$, as in other rotating plasma experiments (LEHNERT, 1971).

These results show that the critical velocity effect is present in VORTEX. Measurements of $n_{\rm e}$ and $T_{\rm e}$ in the flow, using a swept floating double Langmuir probe, show that $n_{\rm e} < 10^{21}~{\rm m}^{-3}$ and $T_{\rm e} > 1~{\rm eV}$ for the range of gases, $p_{\rm O}$, and $B_{\rm Z}$ used. When $B_{\rm Z} < 0.05~{\rm T}$, $n_{\rm e} < 5 \times 10^{20} {\rm m}^{-3}$ due to plasma losses to the walls. Thus $M_{\rm ms} < 1$ when $I_{\rm T} \le 5~{\rm kA}$, since $v_{\rm f} \le v_{\rm C}$.

It is found that $V_T > V_C$ in argon discharges when $I_{\mathrm{T}} > 5 \; \mathrm{kA}$. Oscillograms for an argon discharge, $p_{\mathrm{O}} = 30 \; \mathrm{mtorr}$, $B_{\rm Z}$ = 0.1 T and $V_{\rm B}$ = 10 kV, are shown in Fig.6. The first plateau on the V_{T} trace is the V_{C} value for argon. The second plateau appears superimposed on the first, and approaches the $\,{
m V}_{
m C}\,$ value for hydrogen when $\,{
m I}_{
m T} > 20\;{
m kA}$. Similar double-plateau $V_{_{\mathbf{T}}}$ traces were reported by ALFVEN (1960) and ANGERTH et al (1962). The second plateau does not appear for hydrogen or helium discharges in VORTEX, although there is an upward trend for $\,{\rm V}_{\rm T}\,\,$ in these gases for $I_{\mathrm{T}} > 10 \; \mathrm{kA}$. These results are summarized in Fig.7, where the $\mathbf{E}_{\mathbf{R}}$ discharge has been critically damped. The Alfven mach number $M_A = v_f/v_A$ was computed using n_e values from Langmuir probe results, and assuming $v_f \approx E_r/B_z \approx V_T/B_z \cdot (r_2 - r_1)$. This figure shows that $M_A > 1$ is possible for argon if the increase in $\,V_{T\!\!\!\!/}\,$ represents a true increase in v_f .

A high-impedance floating double electric probe was used to measure the radial electric field $E_{\rm r}$ in the flow. The $E_{\rm r}$ values obtained in the centre of the discharge channel (r'=5 cm, r' \equiv r-r $_{\rm l}$) at the midplane (z=0 cm) are shown in Fig.8. The discharge is undercritically damped, with $I_{\rm T}=40~{\rm kA}$ (peak) at $V_{\rm B}=10~{\rm kV}$. Note the similarity of the curves in Fig.7 and Fig.8. The critical value of $E_{\rm r}$ for argon at $B_{\rm Z}=0.1~{\rm T}$ is

$$E_C \approx B_Z \cdot \left(\frac{2 e \varphi_A}{m_A}\right)^{\frac{1}{2}} = 1.2 \times 10^8 \text{ V-m}^{-1}$$

where $\phi_A=25.6\,\mathrm{V}$ and $m_A=6.68\,\mathrm{x}10^{-26}\,\mathrm{kg}$. Thus $E_r>E_C$ for argon when $V_B\geqslant 6.5\,\mathrm{kV}$, for this discharge circuit. The electric fields measured for hydrogen and helium discharges do not exceed their respective critical values.

These results indicate that, for $\rm B_Z=0.1\,T$, only the argon discharge in VORTEX can have $\rm M_{ms}>1$. A study was made of the discharge properties of all three gases, over a range in $\rm B_Z$, $\rm v_B$, and $\rm I_T$, in order to determine the conditions which give the maximum value of $\rm M_{ms}$.

4. OPTIMIZATION

Probe measurements show that $n_{\rm e}$ increases with $I_{\rm T}$, and that $E_{\rm r}$ generally increases with $V_{\rm T}.$ Therefore the maximum discharge power ($V_{\rm B}=10~{\rm kV}$, $I_{\rm T}=40~{\rm kA}$ peak) was used in the optimization. The plasma parameters are insensitive to $p_{\rm O}$ if $10 \le p_{\rm O} \le 100~{\rm mtorr}$, and $p_{\rm O}=30~{\rm mtorr}$ is used as the minimum required neutral density.

It is found that T_e is insensitive to B_Z and m_i , and has a peak value $T_e = 7.0 \pm 1.5 \, \mathrm{eV}$ when I_T is peaked. The temperature increases rapidly with increasing I_T , which suggests that the plasma is ohmically heated.

Electric probe measurements show that, for maximum V_B and I_T , v_f increases with increasing B_Z . These results were confirmed using an upstream-directed DC floating double Langmuir probe, biased to collect saturated ion current. The velocity increases rapidly for $B_Z \leqslant 0.1\,T$, and more slowly for $0.1 < B_Z \leqslant 0.2\,T$. In hydrogen and helium discharges, $v_f < v_C$. This velocity increase is due to the growing azimuthal force (i.e. torque) on the plasma as B_Z increases.

Magnetic probe measurements show that $\rm B_Z$ is unchanged at the centre-midplane position during the discharge, although $\rm \partial B_Z/\partial r > 0$. This result is used together with those presented above to derive the variation of $\rm M_{ms}$ with $\rm B_Z$, shown in Fig.9. The indicated values refer to the time of peak directed plasma flux $\rm (n_e v_f)$ at the centre-midplane. Note that the $\rm M_{ms} < 1$ for hydrogen and helium. Argon discharges have a peak $\rm M_{ms} \approx 2$ at an optimum $\rm B_Z \approx 0.125\,T$. The decrease in $\rm M_{ms}$ for $\rm B_Z > 0.125\,T$ is due to a rapid increase in $\rm v_A$, and only a moderate increase in $\rm v_f$, when $\rm B_Z$ is greater than optimum.

5. ARGON PLASMA FLOW CHARACTERISTICS

Both spatial and temporal variations of the argon flow parameters have been studied. It is found that the flow contains a core of supermagnetosonic plasma, of radial extent ~ 5 cm and height ~ 20 cm, which persists for 200-300 μ s in a quasi-steady phase of the flow.

The rotation has three phases, as shown in Fig.10. Electric probe and directed Langmuir probe measurements at the centre-midplane were used to derive the $v_{\rm f}$ values. An acceleration phase begins at the start of the $E_{\rm R}$ discharge (t=0), and continues to the $I_{\rm T}$ current peak (t $\approx 100\,\mu \rm s$). In this phase the plasma is compressed radially and vertically, and MHD instabilities sometimes occur. A constant-velocity phase follows, for $100 \le t \le 300\,\mu \rm s$, which corresponds to the $I_{\rm T}$ decay time. During this time the plasma is stable, and all parameters are quasi-steady. The third phase, a deceleration and decay period, begins when $I_{\rm T}$ ends. Calculations show that $v_{\rm f}$ decays due primarily to ohmic and viscous losses, at a rate set by the conditions produced in the quasi-steady phase.

Swept and DC measurements from the directed Langmuir probe show that $n_{\rm e}$ and $T_{\rm e}$ vary with time at the centremidplane in a similar way to $v_{\rm f}$. These results are used to derive the time variation of $M_{\rm ms}$ shown in Fig.ll. The flow becomes supermagnetosonic during the acceleration phase,

and $M_{ms}>1$ persists until well into the deceleration phase. The maximum duration of the supermagnetosonic regime is $\approx 300\,\mu s$ at this plasma position, when $B_z=0.125\,T$, $I_T=40\,kA$ (peak), and $V_B=10\,kV$. If $B_z<0.05\,T$, $M_{ms}>1$ cannot be produced in argon using the present E_R discharge circuit.

5.1 Radial Variations

Radial gradients develop in $\ n_e$, T_e , v_f and B_Z during the rotation, due to the centripetal acceleration of the plasma and the loss of plasma to the walls. In the region $0 < r' \le 6 \, \text{cm}$, $\partial n_e/\partial r$ and $\partial B_Z/\partial r$ balance the centripetal force $n_e m_i v_f^2/r$. For $6 < r' \le 10 \, \text{cm}$, $\partial B_Z/\partial r \approx 0$ and $\partial n_e/\partial r < 0$. The classical ohmic diffusion time across the channel is $\tau_D \approx 10^{-8} \, T_e^{\frac{3}{2}} \, (r_2 - r_1)^2 \, \ln \Lambda \approx 120 \, \mu s$ for a typical $T_e = 5 \, \text{eV}$, where $\ln \Lambda$ is the Coulomb logarithm (SPITZER, 1962). Thus $\tau_D < \tau_f$, and cross-field diffusion is an important process. A neutral layer forms at the outer wall, and the neutral pressure gradient balances $n_e m_i \, v_f^2/r$ for $8 \le r' \le 10 \, \text{cm}$.

The electron temperature is uniform for $2 \le r' \le 8$ cm, and has a typical value $T_e \approx 5.5$ eV in the steady rotation. For r' > 8 cm, T_e decays through the neutral layer to zero at the wall. For r' < 2 cm, swept probe measurements of T_e are irreproducible, but all measurements show $T_e > 10$ eV there at the peak $n_e v_f$ time when $I_T > 20$ kA.

This T_e value may be related to the large E_{r} values measured for $r^{\,\prime}<2\;cm$ when V_{τ} and I_{τ} are high.

Figure 12 shows the v_f midplane radial profile. Electric probe measurements give $E_{\rm r} > 6 \times 10^3 \; \rm V \; -m^{-1}$ at r' = 1 cm when $B_z = 0.1 \text{ T}$, $V_B = 10 \text{ kV}$, and I_T is peaked at 40 kA. This observation is interpreted as the detection of a space-charge sheath near the inner electrode (anode). A similar observation was reported by ØSTER (1969). Such sheaths can form in rotating plasmas when n_e/B_Z is sufficiently small (EBEL and TREIMAN, 1959; LONGMIRE, 1963), and result from the difference in the ion and electron mobilities across B2. It is found that the sheath forms in VORTEX argon discharges at $\,{\rm B}_{_{\rm \!Z}}={\rm O.1\,T}\,$ when centrifugal forces reduce n_e below $5 \times 10^{19} \text{m}^{-3}$ near r' ≈ 0, provided the radial current density approaches $j_r = e n_e C_s$ there. This suggests that the E_r and T_e values near the anode may be connected with a currentdriven cross-field instability (see BARRET et al, 1972), although the results are preliminary.

The radial variation of M_{ms} at $B_z=0.1\,\mathrm{T}$ is shown in Fig.13. Note that $M_{ms}>1$ far from the walls. For $r'>7\,\mathrm{cm}$, low values of v_f , probably due to viscous drag, prevents $M_{ms}>1$.

5.2 Vertical Variations

The parameters T_e , B_Z , and v_f are essentially uniform over the channel height, to within 1cm of the end insulators. When V_T approaches the V_C value for hydrogen, measurements of E_r and T_e near the end insulators become irreproducible, and high-frequency noise $(w>10^7 \, {\rm s}^{-1})$ appears on the V_T , E_T and B_Z oscillograms (see ANGERTH et al, 1962). Similar effects are observed in hydrogen and helium discharges when $V_T \approx V_C$ for those gases, which suggests that the critical velocity effect is responsible for the fluctuations.

Vertical plasma pinching is observed when $\rm\,I_T>10-15\,kA$, depending on the $\rm\,B_Z$ value. The pinching begins simultaneously with the rise in $\rm\,V_T$ above the $\rm\,V_C$ level for argon. At the $\rm\,E_R$ start time (t_1) , $\rm\,n_e\approx2\times10^{20}\,m^{-3}$ for $-14\leqslant z\leqslant14$ cm at $\rm\,B_Z=0.1\,T$, where z is the vertical position measured from the midplane. At $\rm\,t_z$, the peak $\rm\,I_T$ time $(t_2\approx100\,\mu s)$, $\rm\,n_e\approx4\times10^{20}\,m^{-3}$ for $-12\leqslant z\le12$ cm and $\rm\,n_e\approx2\times10^{20}\,m^{-3}$ near the insulators. Pinching continues during the constant-v_f flow phase, as shown in Fig.14. Here $\rm\,t_3\approx150\,\mu s$, $\rm\,t_4\approx275\,\mu s$, $\rm\,B_Z=0.1\,T$, and $\rm\,V_B=10\,kV$. For $\rm\,t>t_4$, the vertical $\rm\,n_e$ profile again becomes more uniform, and $\rm\,n_e$ decreases in the deceleration phase of the flow.

The asymmetry in $\rm\,n_{e}\,$ shown in Fig.14 results in a non-uniform $\rm\,M_{ms}\,$ vertical profile, as shown in Fig.15

 $(B_Z=0.1\,\mathrm{T})$. The region $9\leqslant z \le 15\,\mathrm{cm}$ has $M_{\mathrm{ms}} < 1$ at all times. These asymmetries may be due to a nonuniform distribution of j_{r} , as I_{T} follows the minimum inductance path through the plasma. However, the data is insufficient to uniquely determine the causes for the asymmetry.

5.3 Stability

Magnetic probe measurements show that the argon flow is hydromagnetically stable during the constant-velocity and deceleration phases of the flow. This stability is attributed to Coriolis forces, finite gyro radius effects, and radial gradients in $n_{\rm e}$ and $B_{\rm z}$.

The region $0 < r' \le 6 \text{ cm}$ is stable against the Rayleigh-Taylor interchange mode since $\partial n_e/\partial_r > 0$ and $\partial B_Z/\partial_r > 0$ (MILANTIEV and ØSTER, 1969). This is a result of flux-conservation by the electrodes. The outer region 6 < r' < 10 cm is stable against flutes for frequencies $w \leqslant w_{\text{Ci}} = eB_Z/m_i$, and all mode numbers, since

$$2 w_{ci} < v_f \cdot \frac{1}{n_e} \frac{\partial n_e}{\partial r}$$
,

as shown by probe measurements (BARBIAN and RASMUSSEN, 1969). The Coriolis force on the ions provides a restoring force for density perturbations in the radial direction, and the large ion gyro radius $a_i \approx 1-2 \, \mathrm{cm}$ helps to smooth out radial perturbations.

Finite gyro radius effects also stabilize the Kelvin-Helmholtz velocity shear instability. Ignoring viscosity, a sufficient condition for stability against the Kelvin-Helmholtz mode is $\left(\frac{1}{n_e} \ \frac{\partial^n e}{\partial r}\right)^2 > a_i^2 \ ,$

for $w \le w_{\text{Ci}}$ and small mode numbers (ØSTER, 1966). This condition is satisfied in VORTEX.

Fluctuations in B_Z with frequencies $\omega > \omega_{\text{Ci}}$ are sometimes observed in the acceleration phase of the flow, as shown in Fig.16. The lower trace is the field change ΔB_Z measured by a search-coil magnetic probe at r'=8~cm, z=0, for an initial $B_Z=0.1~\text{T}$. The I_T trace is shown for comparison. An instability develops with

$$\omega \approx 7 \times 10^4 \text{ s}^{-1} \approx 3 \text{ } \omega_{\text{Ci}}$$

after the rotation begins, but is damped as $~\rm I_T$ reaches its peak. Phase measurements from electric and magnetic probes indicate that the $~\rm B_Z$ fluctuations are a flute instability at the outer plasma boundary, of mode number $\rm m \approx 12\text{-}15$. It is likely that this interchange mode is stabilized by Coriolis forces, as $\rm v_f$ increases from $\rm \sim 3 \times 10^3 \ m\text{-}s^{-1}$ at the onset of the instability to $\rm \sim 2 \times 10^4 \ m\text{-}s^{-1}$ at the end of the acceleration period.

6. SOLAR WIND SIMULATION

The optimum argon plasma flow ($B_Z = 0.125\,\mathrm{T}$) is used in VORTEX to model some aspects of the interaction of the supermagnetosonic 'quiet' solar wind with the Moon and asteroids. Table 1 gives a comparison of the important dimensionless parameters for these interactions, selected from both the Vlasov and MHD scaling laws (SCHINDLER, 1969). The solar wind parameters are from the review by HUNDHAUSEN (1970). An asteroid radius $R = 25\,\mathrm{km}$ was chosen as an example.

As in all simulations, it is difficult to correctly scale all of the interaction parameters. The principal difficulty in using the VORTEX plasma for solar wind simulation stems from the argon ion mass and the short mean free path in the flow. Since $v_f < 3 \times 10^4 \text{ m-s}^{-1}$, a high mass density is needed to produce $M_{ms} > 1$. This is a direct result of the critical velocity effect, which keeps v_f one order of magnitude smaller than the quiet solar wind flow velocity. Thus the ratio $\lambda_{ei}/a_i \gg 1$ in the solar wind is not preserved in this experiment, where $\lambda_{ei}/a_i < 1$.

Most aspects of the solar wind/Moon interaction are poorly scaled in VORTEX. However, the scaling for the solar wind interaction with a 50 km - diameter asteroid at a heliocentric distance of 2.5 AU is more accurate. Only

TABLE 1

Parameter comparison for three supermagnetosonic plasma interactions. R is the obstacle radius, λ_D is the Debye length, a_e and a_i are the electron and ion gyro radii, respectively, $a_{di} = v_f \cdot w_{ci}^{-1}$ is the directed ion gyro radius, λ_{ei} is the electron-ion mean free path, c/w_{pe} and c/w_{pi} are the electron and ion inertial lengths, respectively, D is the flow scale, β_{th} and β_{dyn} are the thermal and dynamic betas, respectively, and M_s , M_A and M_{ms} are the sonic, Alfven, and magnetosonic mach numbers, respectively.

Parameter	Obstacle in VORTEX argon plasma	Asteroid in solar wind (2.5 AU)	Moon in solar wind (1 AU)
R (m)	5 x 10 ⁻³	2.5 x 10 ⁴	1.74 x 10 ⁶
λ_D/R	1.4 × 10 ⁻⁴	7.7 × 10 ⁻⁴	5.2 × 10 ⁻⁶
a _e /R	1.5 × 10 ⁻²	0.18	1.7×10^{-3}
a _i /R	2-4	3.3	3.5×10^{-2}
a _{di} /R	17	51	0.35
λ _{ei} /R	0.82	~ 107	~ 5 x 10 ⁵
c/w _{pe} R	3.8 x 10 ⁻²	0.19	1.1 × 10 ⁻³
c/w _{pi} R	5	8	4.6 × 10 ⁻²
D/R	8-10	~ 10 ⁹	~ 10 ⁷
^β th	0.12-0.19	0.8	2
^β dyn	6	80	130
M _S	4.7	4.4	3.5
$^{\mathrm{M}}_{\mathrm{A}}$	2	6.3	8
Mms	1.9	4.6	6

the sense of λ_{ei}/R is not preserved, and this discrepancy could be used to advantage. When space probe measurements of asteroid interactions are obtained, a model experiment of this kind may allow the relative importance of a_i and λ_{ei} in the flow features to be determined.

Cylindrical obstacles of 1 cm diameter are inserted into the VORTEX flow with their axes aligned with $\ensuremath{\mathtt{B}_{\mathrm{Z}}}$. Framing camera photographs of the obstacle interactions have been obtained in total light, exposure time lus. Typical photographs for a glass obstacle interaction are shown in Fig.17, where $B_z = 0.125 \,\mathrm{T}$. Four flow regimes are encountered in the course of each discharge, as the flow parameters change. Comparison of the flow patterns with probe measurements in the undisturbed flow shows that a bow wave develops when $M_{ms} > 1$ (Fig.17c). The propagation angle of the luminous front corresponds to a mach number ~2, in good agreement with $\,{\rm M}_{\rm \!mS}\,\,$ values derived from probe results. This suggests that the bow wave may be a perpendicular hydromagnetic shock. No measurements have been made of the disturbed plasma parameters near the obstacles, so that the flow patterns have not been compared in detail with MHD and shock wave theories.

Induced currents have been detected in a graphite obstacle by means of a Rogowski coil buried in the graphite (SRNKA, 1973b). The current is induced by the motional

electric field $E_{\rm r}$. A similar induction process may have an important role in the interaction of stellar winds with Moon-like objects (SONETT and COLBURN, 1968; SONETT et al, 1970).

7. CONCLUSIONS

Results from this experiment show that supermagnetosonic flows can be produced using a quasi-steady rotating argon plasma. When the discharge current and voltage are sufficiently large, the plasma is pinched away from the end insulators cut by the magnetic field lines, and the flow velocity increases as the radial voltage across the discharge tube rises. The pinching force is due to the azimuthal current j_{θ} in the plasma, which arises from the difference in drift velocities of the ions and electrons in the presence of the centripetal acceleration. It is j_{θ} which produces the $\partial B_{\mathbf{Z}}/\partial \mathbf{r}$ force that partly balances the centripetal force on the plasma.

The flow velocity exceeds the value predicted for argon by the critical velocity theory, but is always less than the critical velocity for hydrogen. This effect may be due to the presence of hydrogen in the flow, outgassed from the chamber walls during the discharge. Lighter gases should collect near the insulator surfaces, due to centripetal accelerations and ion-ion collisions (LEHNERT, 1971), and the limiting voltage of the discharge may be

determined by the properties of the lighter species.

ANGERTH et al (1962) have shown that the second plateau on the discharge voltage for heavy gases, which approaches the limiting hydrogen value, can be removed by baking the electrodes to remove water vapour and absorbed hydrogen. It is not known whether $v_f > v_C$ was achieved in their experiment when $V_T > V_C$, or if $v_f \approx v_C$ after baking. If this is the case, the flow characteristics could be those of a hydrogen plasma interacting with both argon plasma and neutral hydrogen at the end insulators. A model for the critical velocity effect in multi-component plasmas does not exist, and the VORTEX electrodes are not bakeable, so that further discussion of this effect is speculative. However, it is clear that if the ions are sufficiently massive, so that their diffusion rate to the insulators is low, and if the discharge current is sufficiently large, so that some vertical plasma pinching occurs, then the plasma/neutral interaction is weakened (i.e. momentum losses are reduced) and $v_f > v_C$ can be produced.

The supermagnetosonic flow in VORTEX could be used in a number of investigations. One interesting experiment is the laboratory simulation of the solar wind flow near asteroids and other small bodies in the solar system.

REFERENCES

- ALFVEN, H. (1954), 'On the Origin of the Solar System'.
 Oxford University Press.
- ALFVEN, H. (1960), Rev. Mod. Phys., 32, 710.
- ANDERSON, O.A., BAKER, W.R., BRATENAHL, A., FURTH, H.P.

 ISE, J., KUNKEL, W.B. and STONE, J.M. (1958),

 Proc. 2nd Int. Conf. on the Peaceful Uses of Atomic
 Energy, 32, 155.
- ANDERSON, O.A., BAKER, W.R., BRATENAHL, A., FURTH, H.P. and KUNKEL, W.B. (1959), J. Appl. Phys., 30, 188.
- ANGERTH, B., BLOCK, L., FAHLESON, U. and SOOP, K., (1962),
 Nuclear Fusion, S62, part 1, 39.
- BARBIAN, E.P. and RASMUSSEN, C.E., (1969), Plasma Phys., 11, 197.
- BARRET, P.J., FRIED, B.D., KENNEL, C.F., SELLEN, J.M. and TAYLOR, R.J. (1972), Phys. Rev. Lett., 28, 337.
- BONNEVIER, B., (1971), Plasma Phys., 13, 763.
- DANIELSSON, L., (1970), Phys. Fluids, 13, 2288.
- EBEL, M.E. and TREIMAN, S.B. (1959), Los Alamos report LA-2408, 16.
- HALBACH, K., BAKER, W.R. and LAYMAN, R.W., (1962),
 Phys. Fluids, 5, 1482.
- HUNDHAUSEN, A.J., (1970), Rev. Geophys. Space Sci., 8, 729.
- LEHNERT, B., (1961), Nuclear Fusion, $\underline{1}$, 125.
- LEHNERT, B., (1964), Arkiv for Fysik, 26, 407.
- LEHNERT, B., (1969), Stockholm Report 69-33, Royal Institute of Technology.
- LEHNERT, B. (1971), Nuclear Fusion, <u>11</u>, 485.

- LEHNERT, B., BERGSTROM, J., BURES, M., TENNEFORE, E. and WILNER, B., (1971), 'Plasma Physics and Controlled Thermonuclear Fusion, 1, 59 (IAEA, Vienna).
- LONGMIRE, C.L. (1963), 'Elementary Plasma Physics,'
 Interscience Pub., p.83.
- MILANTIEV, V.P. and OYSTER, F. (1969), Danish AEC report 187, Risö.
- ØSTER, F. (1966), Phys. Fluids, 9, 2529.
- ØSTER, F. (1969), Danish AEC report 191, Risö.
- ØSTER, F. and SILLESEN, A.H. (1972), <u>in</u> Proc. Fifth

 European Conf. on Controlled Fusion and Plasma Physics,

 Grenoble.
- SCHINDLER, K. (1969), Rev. Geophys., 7, 51.
- SHERMAN, J.C. (1969), Stockholm report 69-29, Royal Institute of Technology.
- SONETT, C.P. and COLBURN, D.S. (1968), Phys. Earth
 Planetary Sci., 1, 326.
- SONETT, C.P., COLBURN, D.S. SCHWARTZ, K. and KEEL, K. (1970), Astrophys. Space Sci., 7, 446.
- SPITZER, T., (1962), 'Physics of Fully Ionized Gases', Interscience Pub.
- SPREITER, J.R. and ALKSNE, A.Y. (1970), Ann. Rev. Fluid Mech., 2, 313.
- SRNKA, L.J. (1973a), Ph.D. thesis, University of Newcastle upon Tyne, England.
- SRNKA, L.J. (1973b), <u>in</u> 'Photon and Particle Interactions with Surfaces in Space', R.J.L. Grard, editor,
 D. Reidel Pub. Co.
- VAREY, R.H. (1970), J. Phys. D.: Appl. Phys., 3. 1107

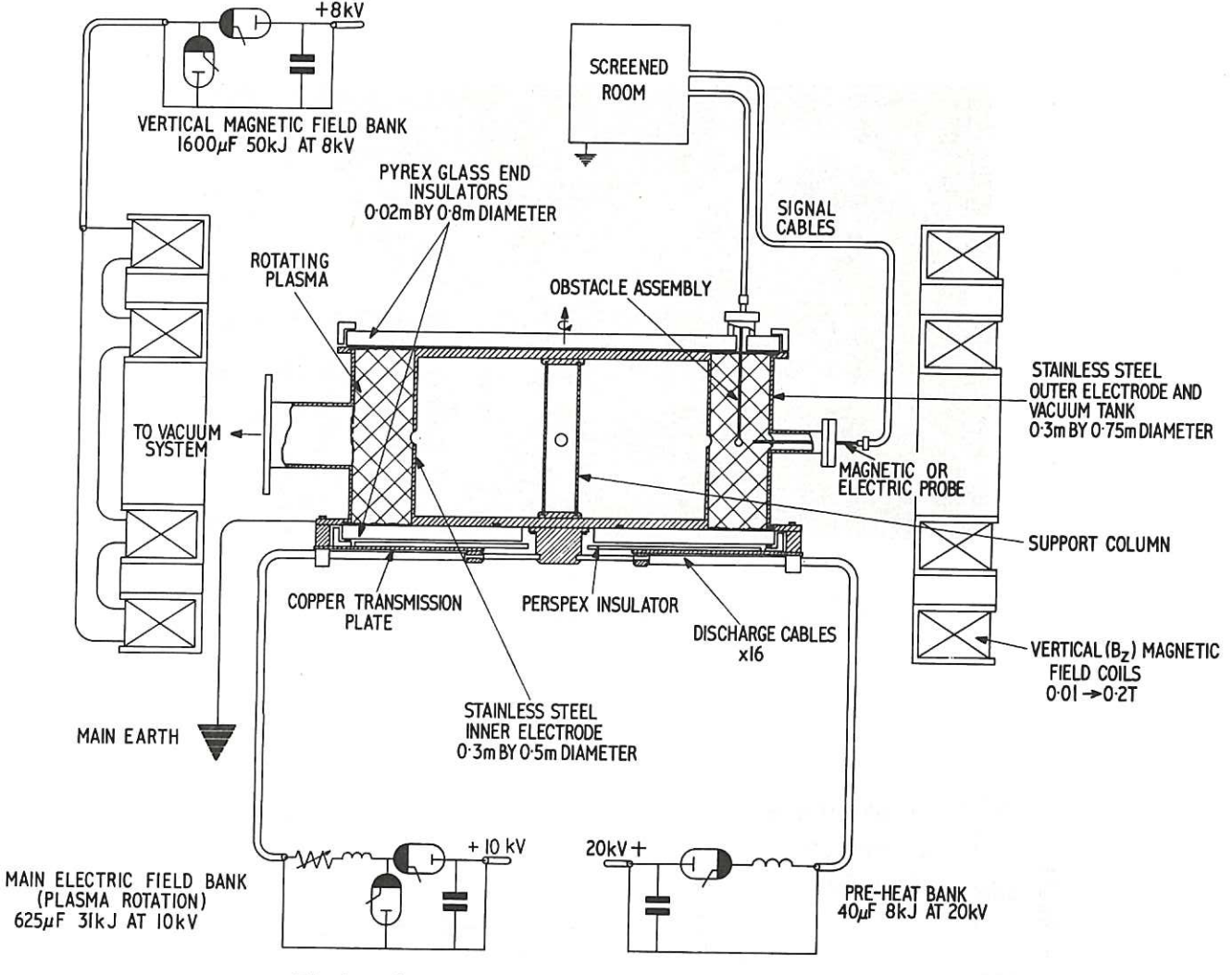


Fig.1 Schematic view of VORTEX rotating plasma experiment.

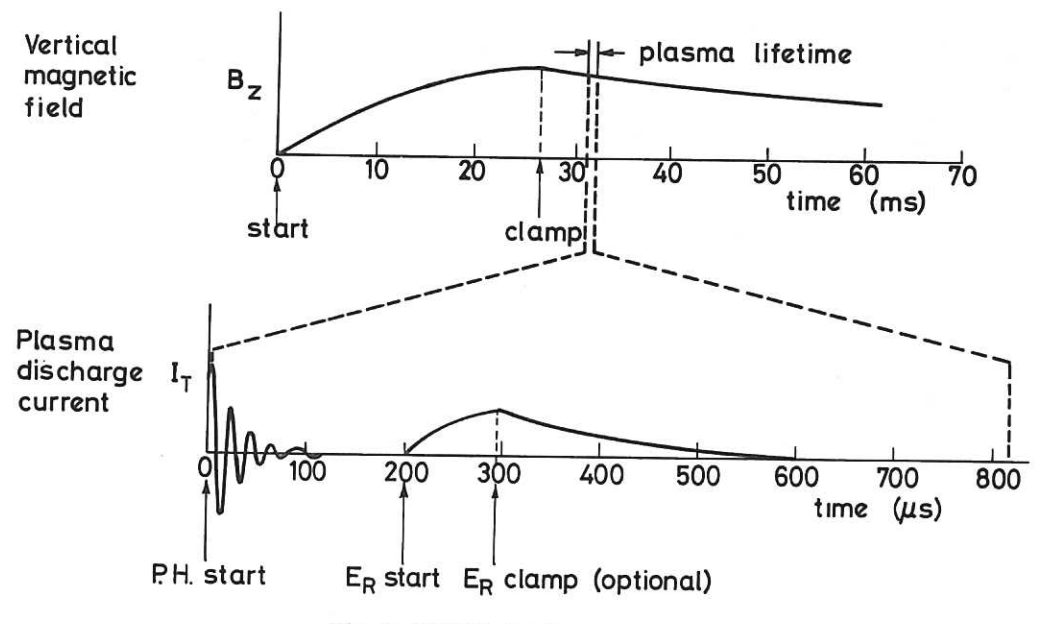


Fig.2 VORTEX discharge sequence. CLM-P 371.

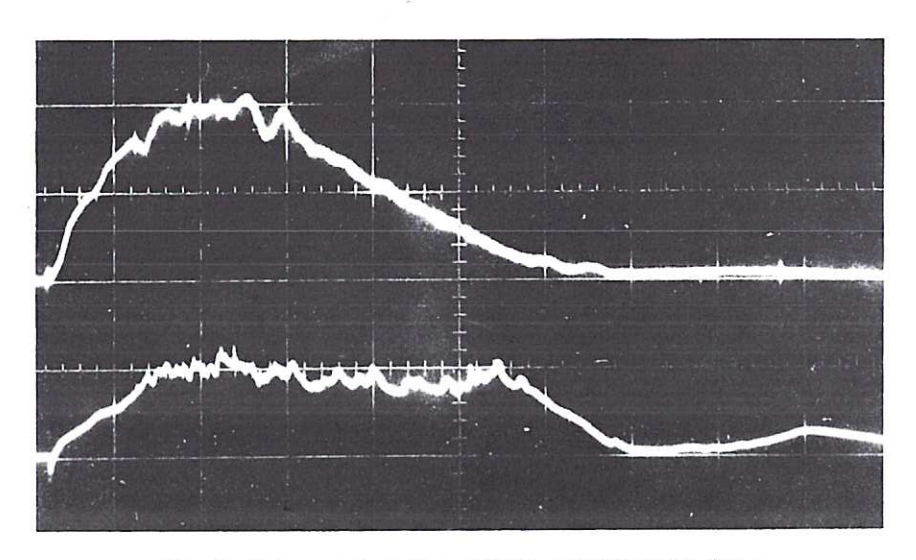
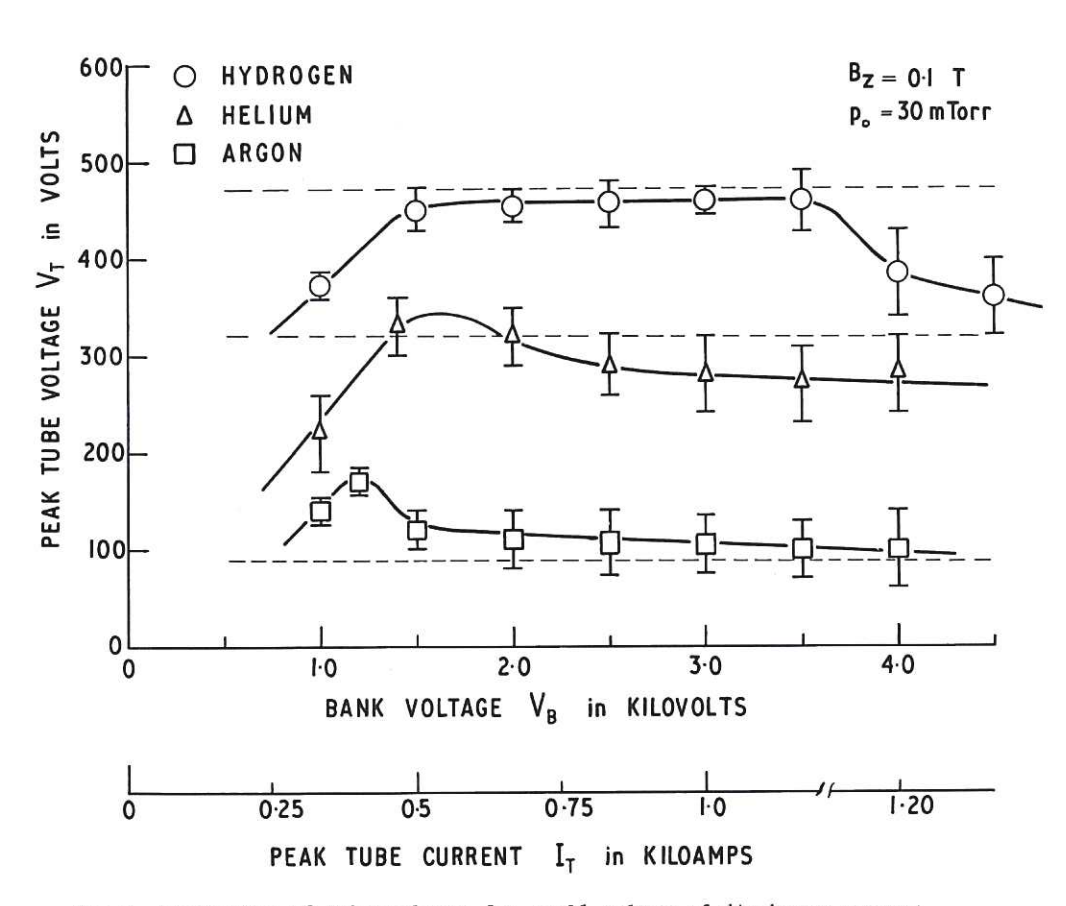


Fig.3 Tube current and voltage oscillograms for a hydrogen discharge. Top trace: I $_{\rm T}$, 500 A/cm, bottom trace: V $_{\rm T}$, 500 V/cm; time base: 50 μ s/cm.



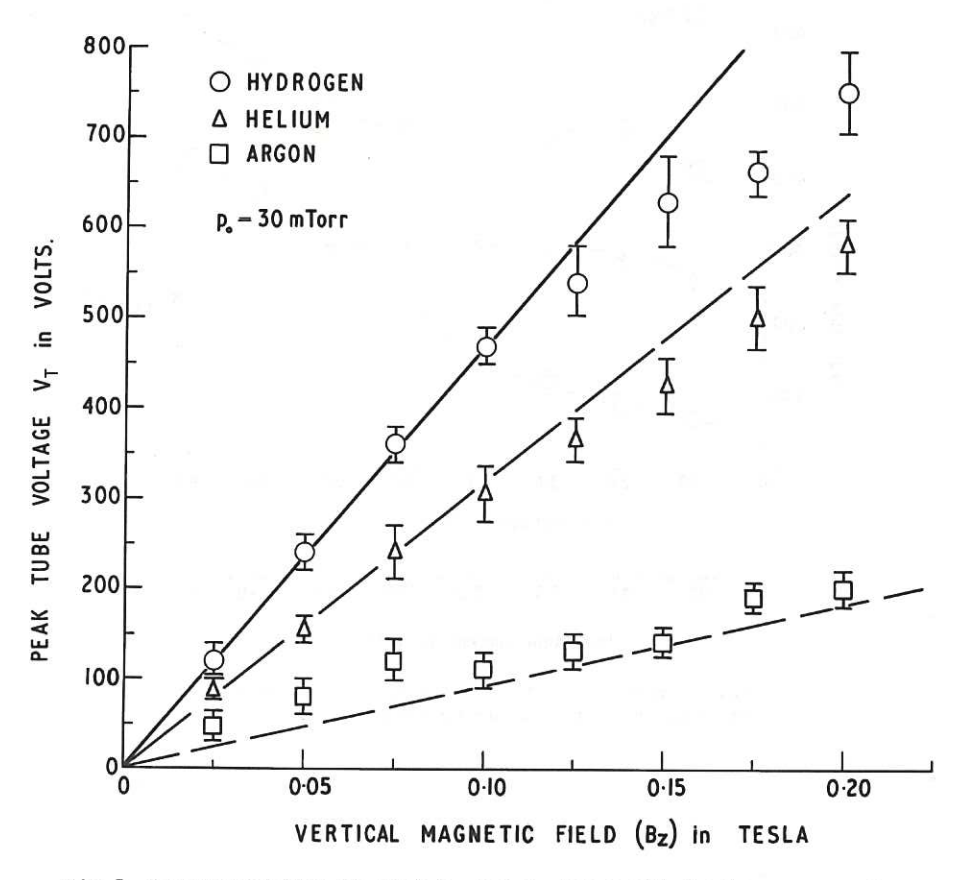


Fig.5 Proportionality of peak V_{T} and $\mathbf{B}_{\mathbf{Z}}$ for small discharge currents.

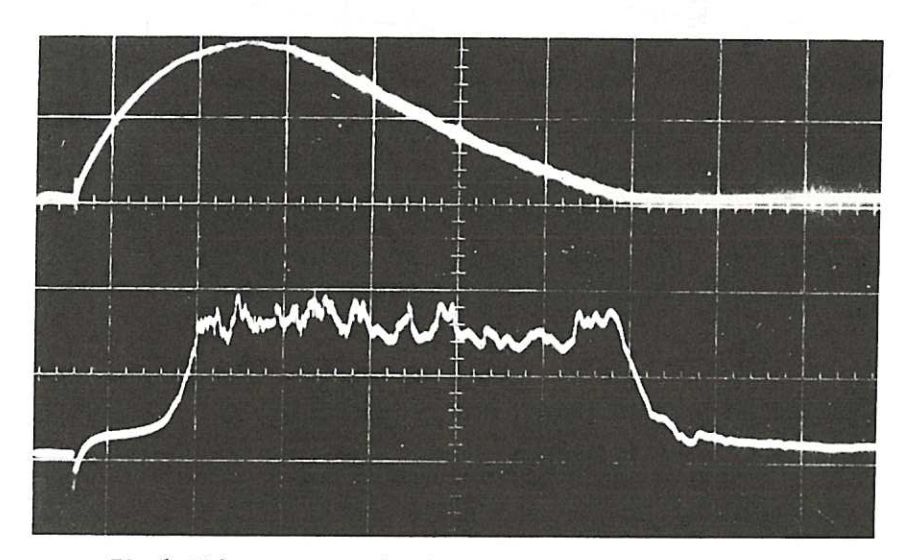


Fig.6 Tube current and voltage oscillograms for an argon discharge, at large I $_T$. Top trace: I $_T$, 20 kA/cm; bottom trace: V $_T$, 250 V/cm; time base: 50 μs /cm. CLM-P 371.

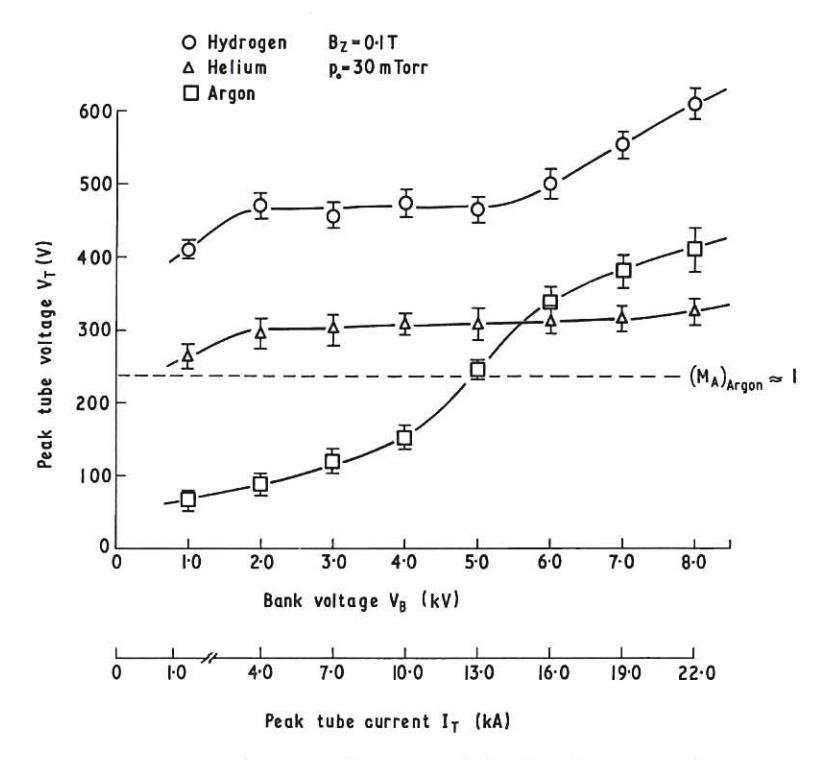


Fig.7 Production of super-critical and supersonic rotating argon plasma using large currents.

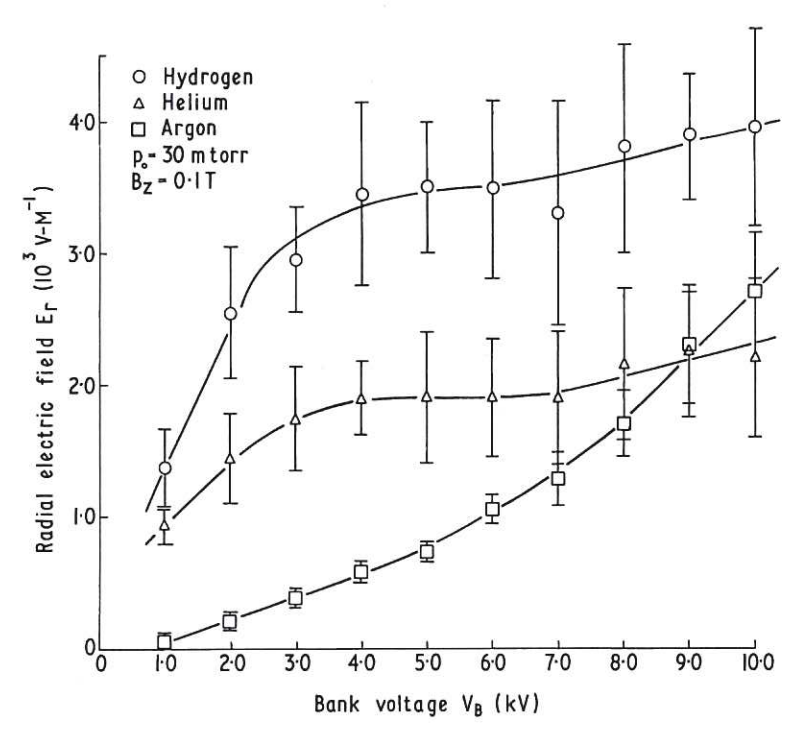


Fig.8 Peak electric fields at the centremidplane in undercritically damped $\rm E_R$ discharges. CLM-P 371.

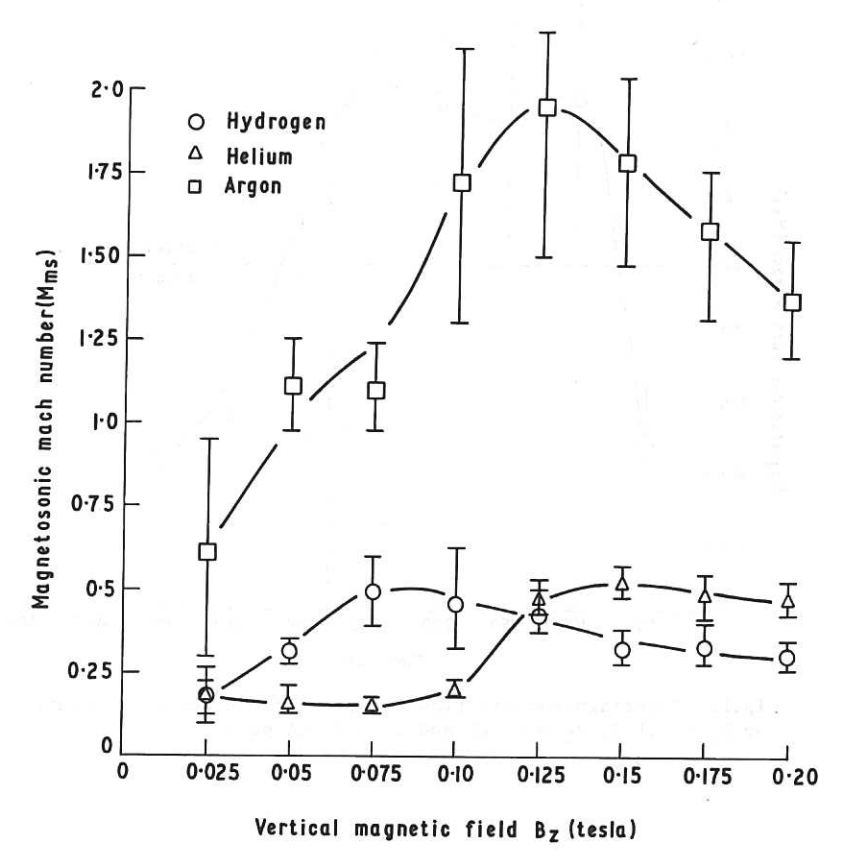


Fig.9 Maximum $\mathbf{M}_{\mathbf{mS}}$ at the centre-midplane position.

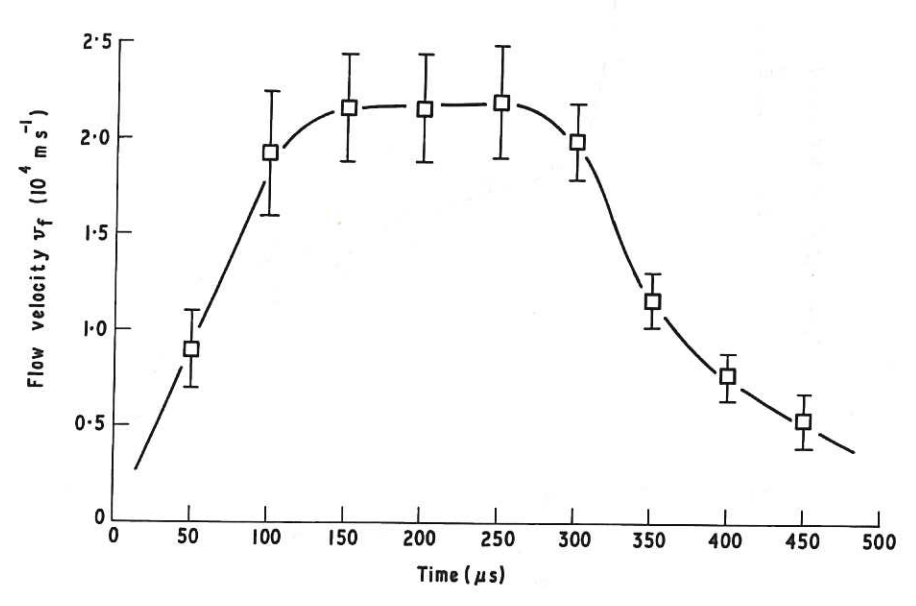


Fig.10 Three phases of the plasma rotation. CLM-P 371.

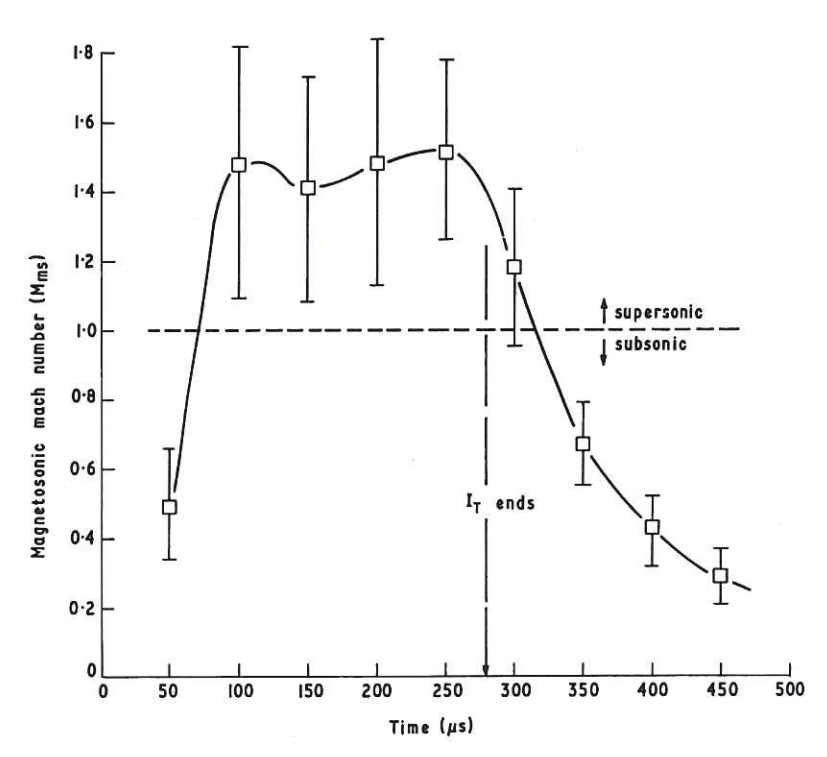


Fig.11 Supermagnetosonic flow duration of the centre-midplane, for B $_{\rm Z}$ = 0.1 T, V $_{\rm B}$ = 10 kV and I $_{\rm T}$ = 40 kA peak.

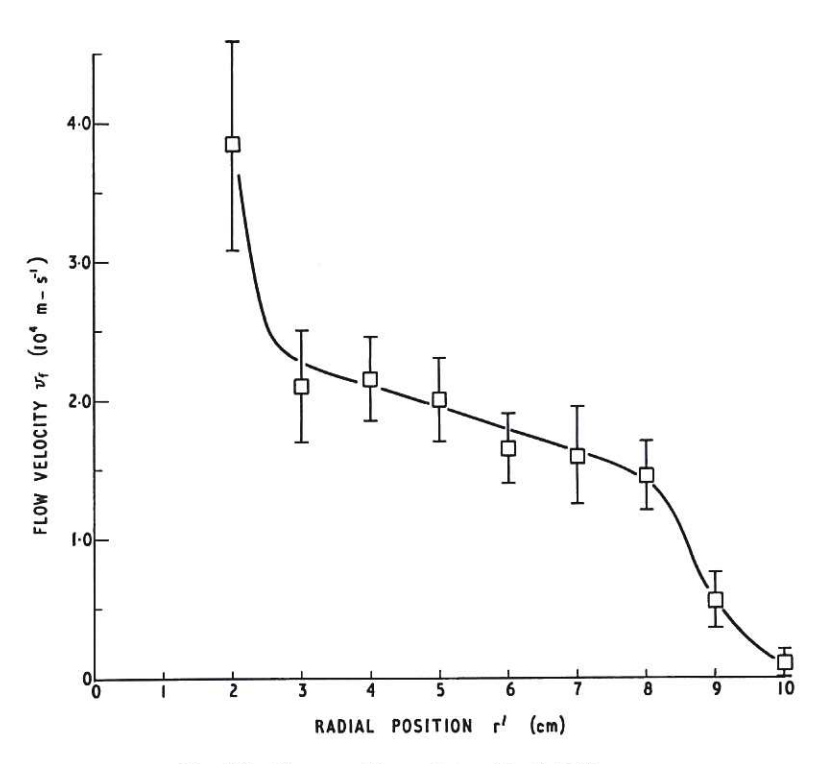


Fig.12 Observation of anode sheath. ${\tt CLM-P~371} \; . \\$

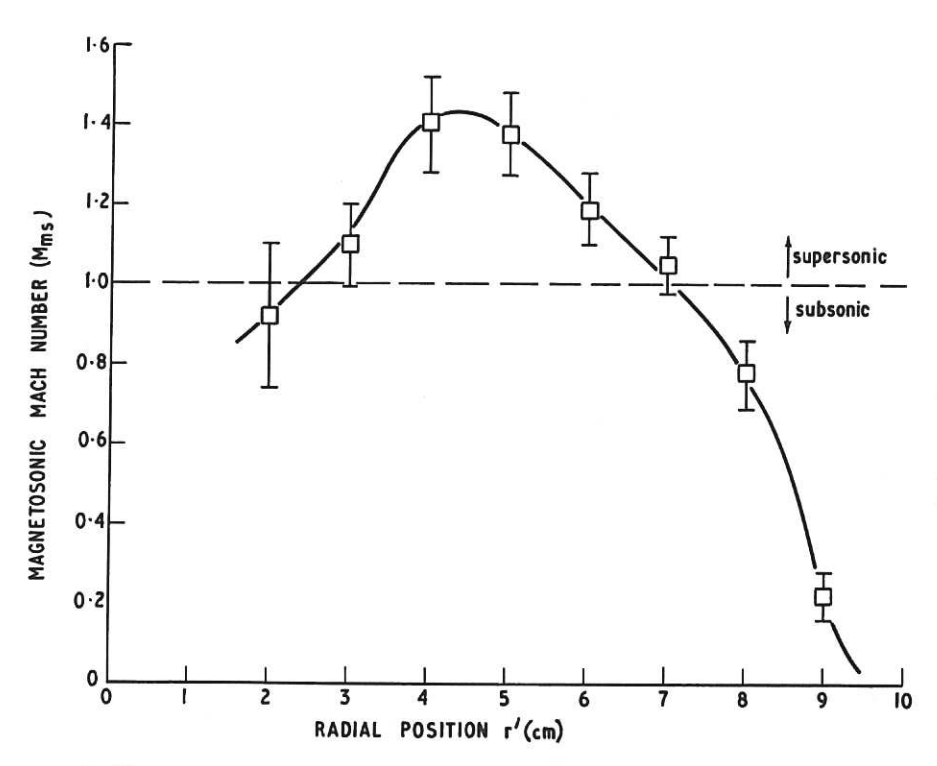


Fig.13 Midplane \mathbf{M}_{ms} radial profile at the peak directed flux time.

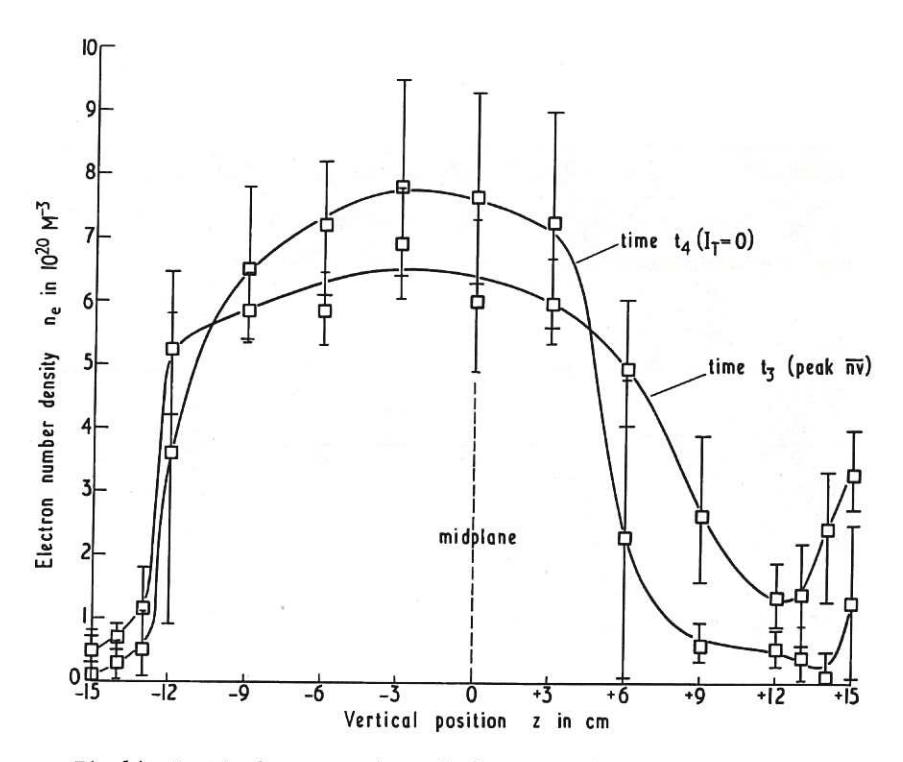


Fig.14 Vertical compression of plasma at the channel centre. CLM-P 371.

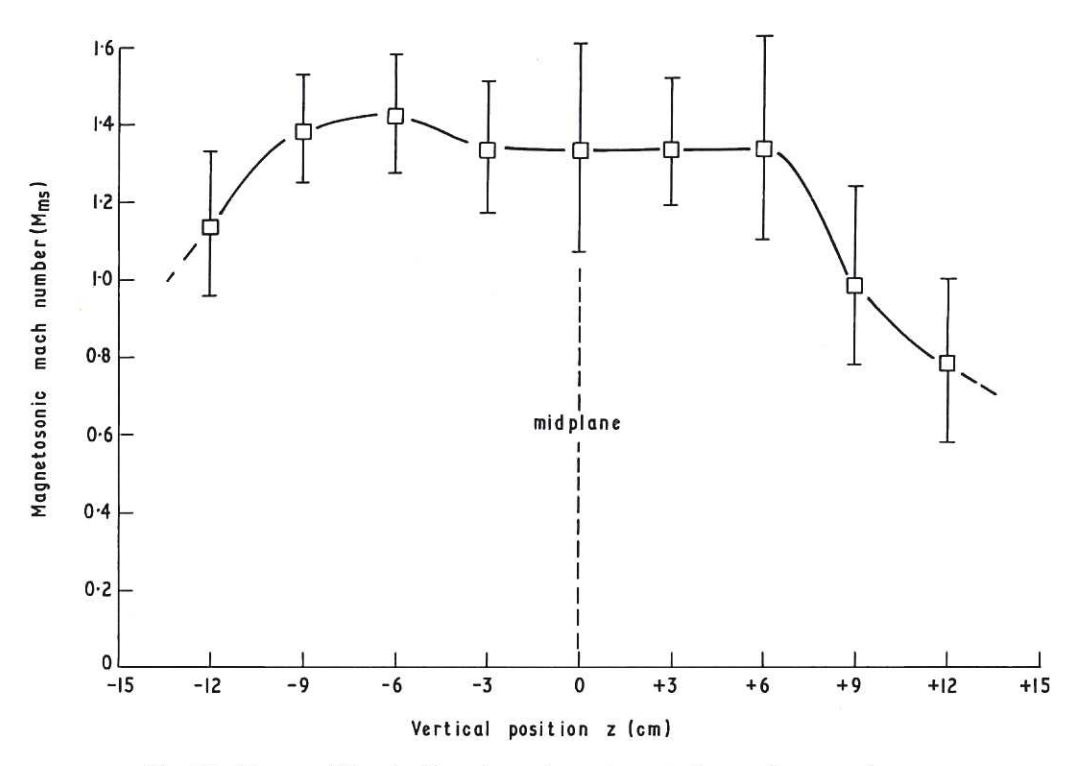


Fig.15 $\,{\rm M}_{\rm ms}$ profile in the channel centre at the peak ${\rm n}_{\rm e} {\rm v}_{\rm f}$ time.

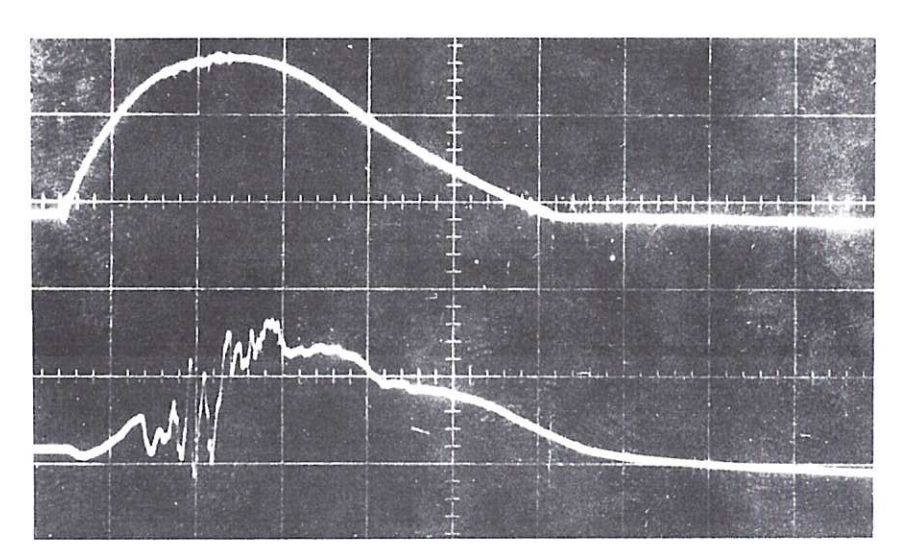
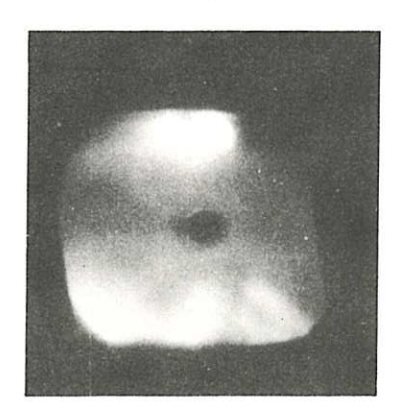
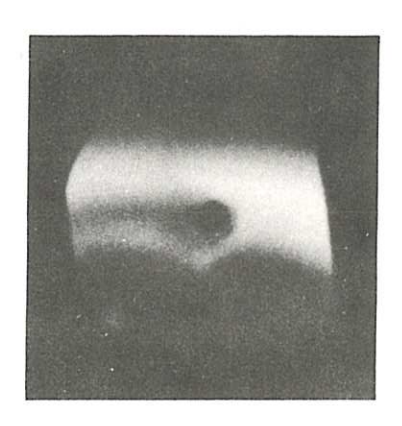


Fig.16 Flute instability with $\omega > \omega_{\text{ci}}$ in the acceleration phase of the rotation. Top trace: I_T , 20 kA/cm; bottom trace: ΔB_z , 5 × 10⁻² T/cm; time base: 50 μ s/div.

CLM-P 371.



(a) sub-magnetosonic



(b) transonic



(c) supermagnetosonic $\mathbf{I_T} \neq \mathbf{0}$



(d) supermagnetosonic $I_{\mathrm{T}} = 0$

Fig.17 Glass obstacle interaction. $\rm B_Z$ is out of the page, the flow is from the right, and the inner electrode is at the bottom of each photograph. CLM-P 371.

*

